ISIJ International, Vol. 53 (2013), No. 2, pp. 375–381

# Effect of Microstructure on Fatigue Strength of Intercritically Austenitized and Austempered Ductile Irons with Dual Matrix Structures

Ismail OVALI,[1)]* Volkan KILICLI[2)] and Mehmet ERDOGAN[2)]

1) Hacettepe Vocational School, Hacettepe University, Beytepe, Ankara, 06800 Turkey. 2) Department of Metallurgical and Materials Engineering, Faculty of Technology, Gazi University, Teknikokullar, Ankara, 06500 Turkey.

(*Received on August 14, 2012; accepted on October 2, 2012*)

In the present study the fatigue strength of austempered ductile irons with dual matrix structures (ADI with DMS) has been studied for an unalloyed ductile cast iron. For this purpose, specimens were intercritically austenitized (partially austenitized) in two phase region ($\alpha + \gamma$) at various temperatures (810°C, 820°C and 830°C) for 20 minutes and then quenched into salt bath held at austempering temperature of 315°C and 375°C for 120 minutes and then air cooled to room temperature to obtain various ausferrite volume fractions and their morphologies. Conventionally austempered specimens (austempered from 900°C) with fully ausferritic matrix and unalloyed as cast specimens having ferrit + pearlite structures were also tested for a comparison. Rotating bending fatigue test were carried out an the experimental results showed that, in ADI with DMS, volume fraction of ausferrite and continuity of ausferritic structure along intercellular boundaries play important role in determining fatigue strength. The fatigue strength of these specimens increases with increasing ausferrite volume fraction. The fatigue strength was correlated with the ausferrite volume fraction and high carbon austenite and its carbon content. Conventionally austempered specimens exhibited much greater fatigue strength than ADI with DMS specimens.

KEY WORDS: austempered ductile iron; dual matrix structure; fatigue; ausferrite volume fraction.

## 1. Introduction

In the newly developed ductile cast iron with dual matrix structure,[1–20)] the structure consists of proeutectoid ferrite, and ausferrite (bainitic ferrite and high carbon austenite (it is also called retained, stable or transformed austenite) or martensite. Therefore it is also called Dual Matrix Structure (DMS).[1–11)]

Austempered ductile iron (ADI) with DMS has been found to be validated for suspension parts of the automotive, owing to its greater ductility than the conventionally heat treated austempered ductile iron. This material showed tensile and proof stress, together with hardness, similar to pearlitic grades, and ductility at the same level as ferritic grades.[1–4)]

The fatigue properties of ductile iron and ADI have been studied by many investigators and several studies have been reported the relationship between fatigue strength and austempered microstructure.[21–41)] The fatigue strength of ADI was superior to those of ferritic, pearlitic and quenched and tempered grades.[21,34–37)] The literature on fatigue properties of ADI presents that the chemical composition, austenization and austempering temperatures are important parameters to control of the fatigue strength of ADI.[21–41)]

Authors had examined the phase transformations, microstructure, mechanical properties (tensile and hardness) and wear behavior of ADI with DMS comprehensively.[4–20)] Fatigue properties of ADI with DMS matrix was studied by Verdu *et al*.[41)] reported prior to 2005. They produce DMS matrix in ADI using short austenization time (incomplete austenization) following by austempering in their research. Researchers emphasized that the dual matrix ADI having considerable higher fatigue properties than as cast ductile cast irons.[42)]

No efforts have so far been made to optimize the fatigue properties of ADI with DMS by controlling the proeutectoid ferrite (PFVF) and ausferrite volume fraction (AFVF) by austempering from intercritical austenization temperature (ICAT) range.

In the present study, the influence of an ICAT of 810°C, 820°C and 830°C and a conventional austenitizing temperature of 900°C and different austempering temperatures (315°C and 375°C) on microstructure and fatigue properties of unalloyed ductile iron has been investigated.

## 2. Experimental Details

The chemical composition of as cast unalloyed ductile iron used in the present study is given in **Table 1**.

The ductile iron was produced in a medium frequency induction furnace in a commercial foundry. The tundish cover ladle method was used to treat a 500 kg melt of iron with 6–7%Mg containing ferrosilicon alloy at 1 450°C.

* Corresponding author: E-mail: iovali@hacettepe.edu.tr
DOI: http://dx.doi.org/10.2355/isijinternational.53.375

**Table 1.** Chemical composition of unalloyed ductile iron (wt.-%).

| C | Si | Mn | P | S | Mg | Cr | Ni | Mo |
|---|---|---|---|---|---|---|---|---|
| 3.59 | 2.875 | 0.402 | 0.0245 | 0.0115 | 0.041 | 0.0235 | 0.0215 | <0.01 |
| Cu | Al | Ti | V | Nb | W | Co | Sn | Fe |
| 0.067 | 0.017 | 0.009 | 0.003 | <0.001 | <0.005 | 0.003 | 0.002 | Rest |

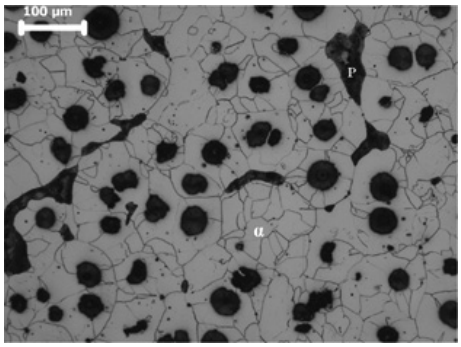


**Fig. 1.** Microstructure of the as cast material (P: Pearlite and $\alpha$: Proeutectoid Ferrite).

Final inoculation was carried out with a 75% ferrosilicon alloy. The melt at the temperature between 1 400 and 1 450°C was cast into Y block sand moulds, which were prepared in accordance with ISO 1083. As cast material had ferrite + pearlite and spheroidal graphite structure (**Fig. 1**).

The preliminary investigation was to determine the dependence of the austenite (martensite at room temperature) volume fraction on intercritical austenitizing temperatures (ICAT). For this purpose, specimens 12 × 12 × 10 mm thick machined from the bottom section of Y-blocks were austenitized for 20 min in air at a series of temperatures from 770 to 850 C (Ae1 and upper critical temperature respectively; see **Fig. 2**) and then quenched into water at room temperature. The subcritical temperature (Ae1) limits were predicted from the empirical formulae of Andrews.[43] Both the subcritical and upper critical temperature limits were obtained experimentally by increasing the intercritical austenitizing temperature from well below the calculated Ae1 temperature to well above upper critical temperature step by step and then water quenching the specimen from these temperatures and measuring the martensite volume fractions. Austenite formed during intercritical austenitizing was assumed to transform to martensite. The martensite volume fraction was determined by point counting on metallographic sections etched in 2% nital. As a result of this preliminary study, three intercritical temperatures of 810, 820, and 830°C, corresponding to 43, 52.5 and 79.8% austenite volume fraction (Fig. 2) were selected for a detailed study of the effect of parent austenite dispersion at ICAT and austempering time on the development of the DMS with different microstructural refinements.

The as cast specimens were intercritically austenitized at the ICAT of 810°C, 820°C, and 830°C for 20 minutes and then rapidly transformed to a salt bath containing 50% $KNO_3$ + 50% $NaNO_3$ held at the 315°C and 375°C for austempering for 120 minutes to produce DMS with different ausferrite volume fractions (AFVF). The austempering time 120 min were selected because of the previous studies showed that the optimum tensile and ductility combinations

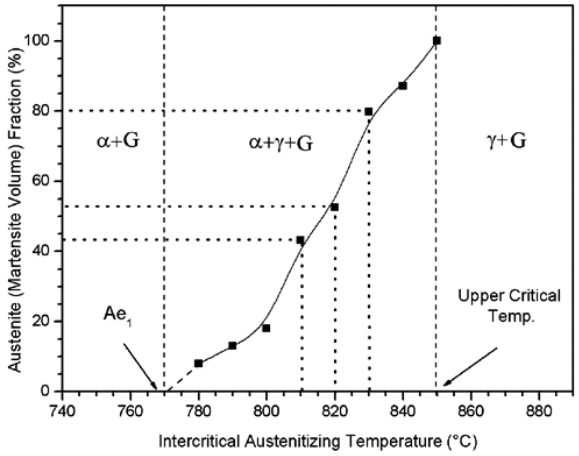


**Fig. 2.** Dependence of the austenite volume fraction on intercritical austenitizing temperature.

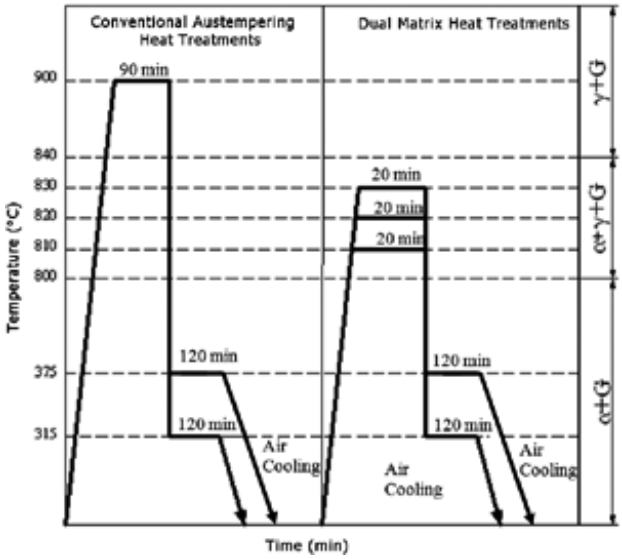


**Fig. 3.** Summary of heat treatments.

of ADI with DMS obtained this austempering time.[4,5,9,10] It may be interpreted as a useful range or process window for present ADI to obtain ideal ausferritic structure.

As cast specimens were also heat-treated at the conventional austenitizing temperature of 900°C for 90 min and then austempering at the same austempering temperature for comparison. **Figure 3** provides a summary of heat treatments. Throughout these heat treatments, the temperature of each specimen was monitored by a thermocouple spot-welded to the centre of one of its faces.

The relative amounts of the high carbon austenite and total ferrite volume fractions in all heat treated specimens were measured by X-Ray diffraction following the standard procedure.[44,45] X-ray diffraction profiles were obtained on a Brucer D8 X-ray diffractometer at 40 kV and 20 mA using monochromated Cu K$\alpha$ radiation ($\lambda$ = 1.54056 A°). The specimens were scanned in the 2$\theta$ range of 40–100° at a scanning speed of 0.05°/min. The integrated areas of both austenite (220) and (311) and ferrite (211) peaks were used for determination of volume fraction of austenite and ferrite. The carbon concentration in the austenite was calculated from its lattice parameter using a relationship of Roberts.[46]

The ausferrite volume fraction (AFVF) and proeutectoid

**Table 2.** Result of metallographic investigations and fatigue strengths.

| Specimen Code | Austempering Temperature (°C) | Ausferrite volume fraction[1] (vol.-%) | Proeutectoid volume fraction[1] (vol.-%) | Graphite volume fraction[1] (vol.-%) | High-carbon Austenite volume fraction[2] ($X_\gamma$) (vol.-%) | Austenite Carbon content[2] ($C_\gamma$) (wt.-%) | ($X_\gamma$ $C_\gamma$) | Fatigue strength (MPa) |
|---|---|---|---|---|---|---|---|---|
| As-cast | – | 5.5 * | 82.3 | 12.2 | – | – | – | 230 |
| 810-375 | 375 | 40.4 | 47.4 | 12.2 | 5.9 | 1.295 | 0.076 | 350 |
| 810-315 | 315 | 22.6 | 65.2 | 12.2 | 3.8 | 1.263 | 0.048 | 325 |
| 820-375 | 375 | 47.7 | 40.1 | 12.2 | 8.3 | 1.347 | 0.112 | 375 |
| 820-315 | 315 | 30.9 | 56.9 | 12.2 | 6.4 | 1.305 | 0.084 | 350 |
| 830-375 | 375 | 70.9 | 16.9 | 12.2 | 14.5 | 1.529 | 0.222 | 400 |
| 830-315 | 315 | 54.9 | 32.9 | 12.2 | 10.9 | 1.416 | 0.154 | 380 |
| 900-375 | 375 | 87.8 | – | 12.2 | 35.5 | 1.976 | 0.701 | 450 |
| 900-315 | 315 | 87.8 | – | 12.2 | 29.8 | 1.817 | 0.541 | 425 |

[1] Point counting measurements
[2] X-RD measurements
* Pearlite volume fraction

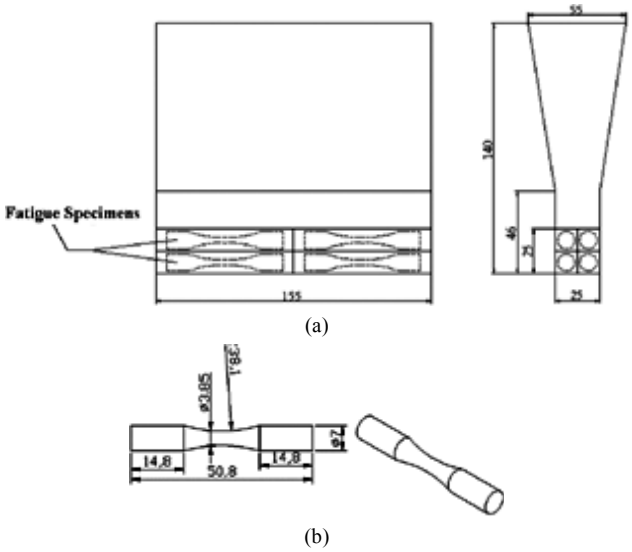


**Fig. 4.** a) Y Block, b) Fatigue Specimen (Dimensions in mm).

ferrite volume fraction (PFVF) calculated by point counting on etched (2% nital) metallographic sections. The results of microstructural constituent proportions are listed in **Table 2**. Between 1 000 and 2 000 points were counted to keep the standard error of the volume fraction of phases below 6%. The nodule count and the nodularity were measured 210 $mm^{-2}$ and 94% respectively.

Specimens are coded according to austenitizing temperature and austempering temperature. For example, in specimen code 830-375, 830 stands for austenitizing temperature and 375 corresponds the austempering temperature.

Following the microstructural studies, fatigue test specimens were machined in accordance with ISO 1143 standard from the bottom section of Y block (**Fig. 4**(a)). Fatigue specimens (Fig. 4(b)) machined after heat treatments to remove any decarburized layer. Metallographic observations showed that similar microstructures produced in 5 mm thick specimens for each series were similar to those produced in the corresponding fatigue test specimens.

After machining the fatigue test specimen, hand polishing was carried out to use fine grades of emery paper vertically followed 3 $\mu$m diamond paste until all circumferential markings were removed. Fatigue tests were carried out at room temperature in air using a rotating bending fatigue machine at a frequency of 3 000 rpm (50 Hz). All tests were performed at a stress ratio of R = minimum stress/maximum stress = –1. At least ten specimens for each heat treated condition were tested at sufficient stress levels to obtain reliable S-N curves and fatigue strengths. The specimen unbroken to $10^7$ cycles showed with arrow in graphics. The fatigue strength of specimens was defined as the highest stress level at which non failure occurred after $10^7$ cycles.

## 3. Results and Discussion

### 3.1. Microstructural Examinations

During austempering process, ADI undergoes a two stage transformation reactions. In the first stage the parent austenite $\gamma$ decomposes into bainitic ferrite $\alpha_b$ and high carbon austenite $\gamma_{hc}$ (retained austenite or transformed stable austenite). During the second stage, this supersaturated high carbon austenite further decomposes into bainitic ferrite and carbides. The desired microstructure of the austempered ductile iron is bainitic ferrite and high carbon austenite, commonly called ausferrite. This desired ausferrite microstructure is obtained at the austempering time interval between end of stage I and at the beginning of stage II reactions. This austempering time interval is called processing window. The ductile cast iron with this desired ausferrite microstructure displays optimum mechanical properties.[3,4,10,16,39,47–51)]

The notable feature of intercritical austenitizing heat treatment comparing conventional austenitizing heat treatment ones is that in the austenite + ferrite region, the austenite volume fraction and its carbon content depends on the ICAT. When the ICAT increases the ausferrite volume fraction and the high carbon austenite volume fraction and its carbon content increases (**Figs. 5** and **6**) and proeutectoid ferrite volume fraction (PFVF) decreases (**Fig. 7**). This result is in good agreement with the existing literature.[4–15)]

Austempering from different ICATs produced a DMS

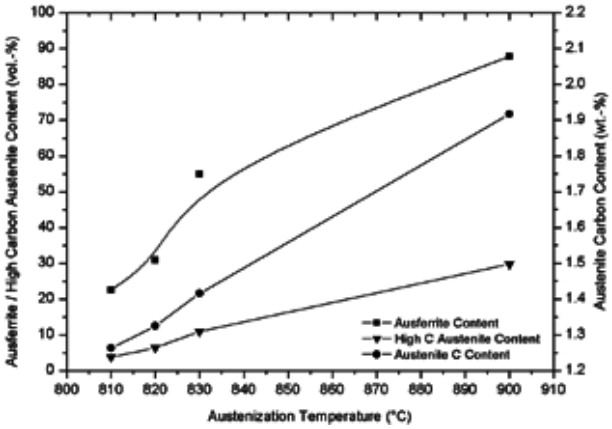


**Fig. 5.** Variation of microstructural constituents and austenite carbon content with austenitization temperatures following austempering at 315°C.

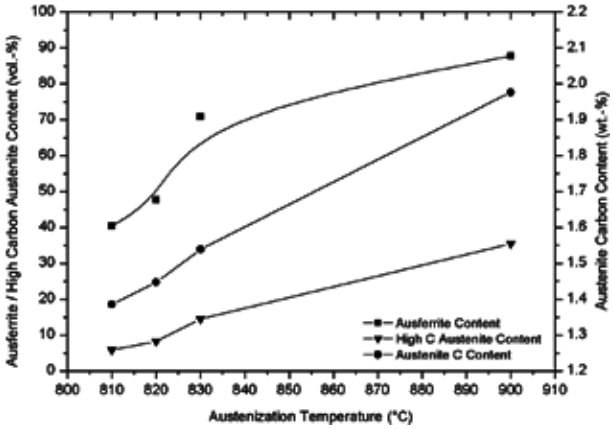


**Fig. 6.** Variation of microstructural constituents and austenite carbon content with austenitization temperatures following austempering at 375°C.

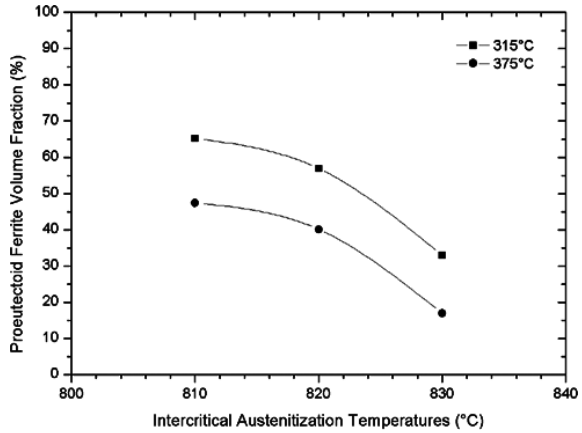


**Fig. 7.** The relationship between proeutectoid ferrite volume fraction and intercritical austenitization temperatures.

consisting of ausferrite + proeutectoid ferrite at the specimens with different AFVFs restricted to eutectic cell boundaries and an isolated or continuous network of ausferritic structure along the eutectic cell boundary formed depending on AFVF (**Figs. 8** to **10**). Eutectic cell boundaries are the potent sites for austenite nucleation.[4,10] AFVF was also depended on austempering temperatures. From the same ICAT austempering at 375°C produced higher AFVF than

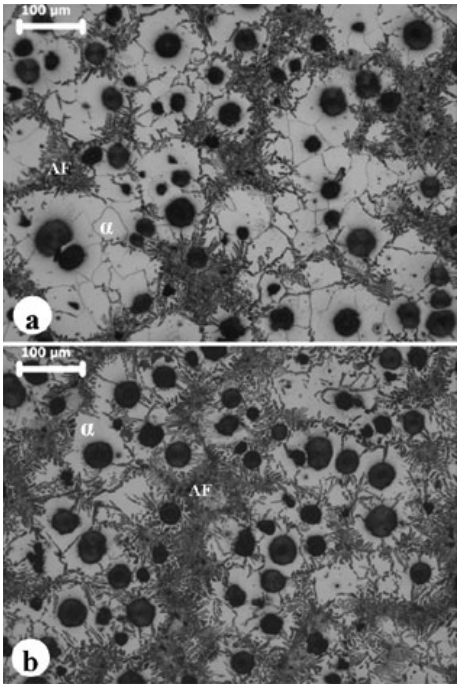


**Fig. 8.** Microstructure of specimens; a) 810-315 and b) 810-375 (AF: Ausferrite and $\alpha$: Proeutectoid Ferrite).

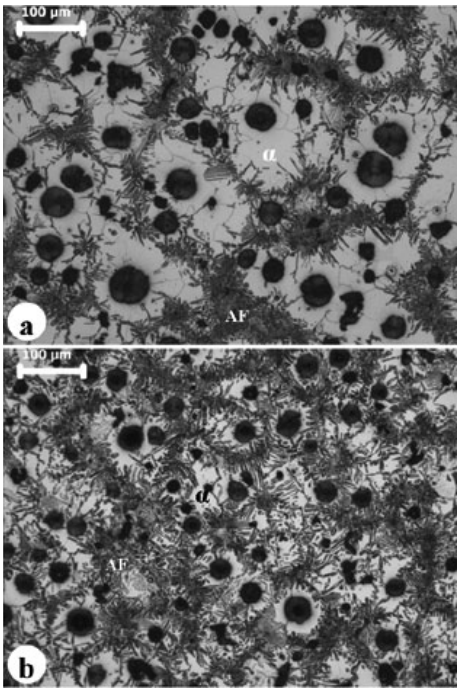


**Fig. 9.** Microstructure of specimens; a) 820-315 and b) 820-375 (AF: Ausferrite and $\alpha$: Proeutectoid Ferrite).

austempering at 315°C (Figs. 8 to 10).

Conventional austempering heat treatment of ADI involves heating the ductile iron up to 875–925°C (in this study 900°C) and then rapidly cooling to the austempering temperature and holding at this temperature for various times and then air cooling to room temperature. Microstructure of conventional austempered specimens were showed in **Fig. 11**. In the conventionally austempered specimen 900 (87.8 AFVF), austempering for 120 min produced a typical ausferritic structure throughout the specimen without mar-

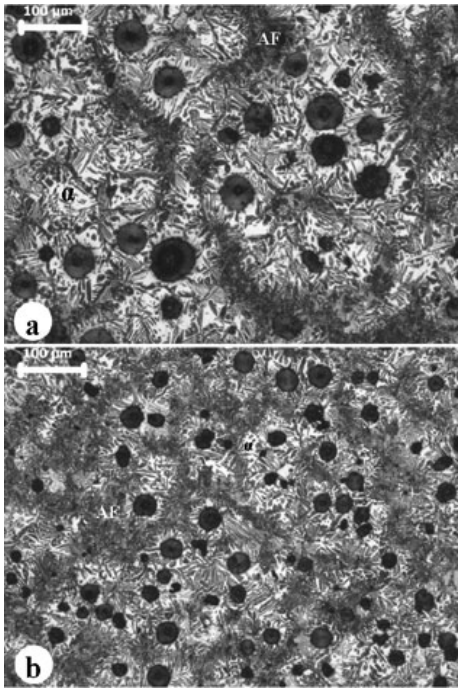


**Fig. 10.** Microstructure of specimens; a) 830-315 and b) 830-375 (AF: Ausferrite and $\alpha$: Proeutectoid Ferrite).

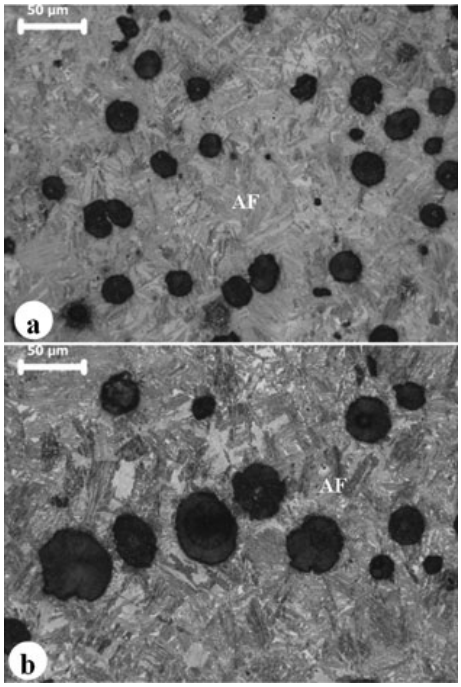


**Fig. 11.** Microstructure of specimens; a) 900-315 and b) 900-375 (AF: Ausferrite).

tensite (Fig. 11).

Some alloying elements like Si and Mn are inherently present in ADI. It is already known that Si concentrates near a graphite nodule and Mn partitions into a eutectic cell boundary.[16] Mn reduces the activity of carbon and encourages austenite nucleation (an austenite stabilizer). Therefore it is reasonable to assume that eutectic cell region is the most potent site for austenite nucleation. The reason for the absence of formation of austenite near graphite nodules may be attributable to the effect of Si segregation on the reduction of the austenite formation rate.[16]

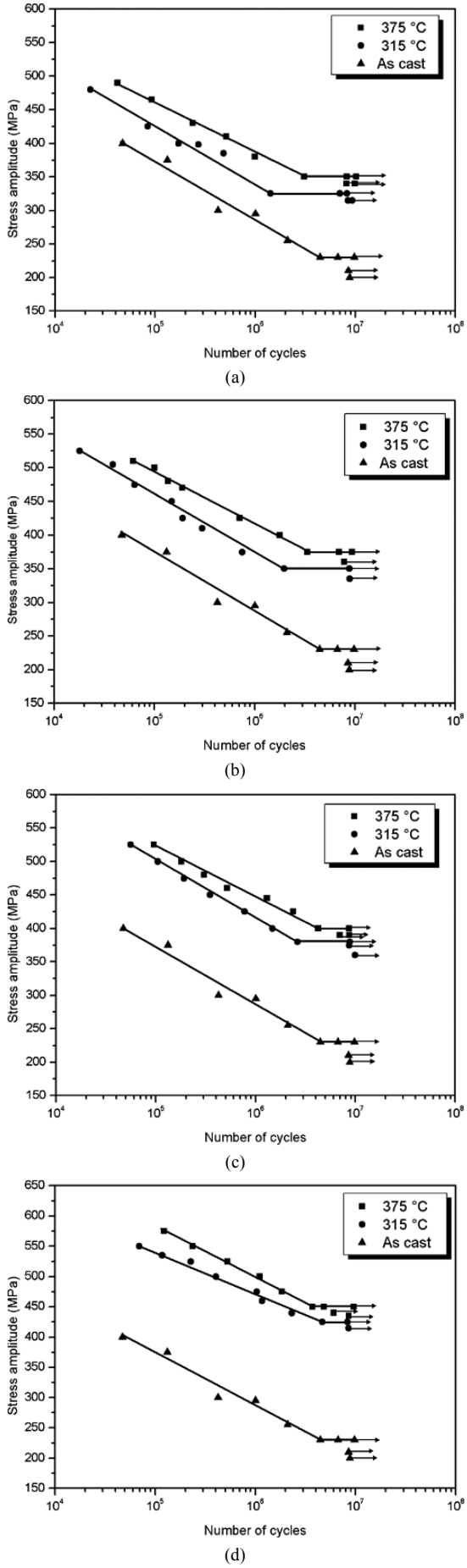


**Fig. 12.** S-N curves of specimens; a) 810-315 and 810-375, b) 820-315 and 820-375, c) 830-315 and 830-375, d) 900-315 and 900-375.

### 3.2. The Fatigue Properties of ADI with DMS

The S-N curves of tested specimens are given in **Fig. 12**. The experimental results showed that the fatigue strength of specimens reflects the variations in microstructures. As cast specimen having fully ferritic matrix (Fig. 1) exhibited the lowest fatigue strength compared to the other tested specimens (Figs. 12(a) to 12(d)).

Fatigue strengths of ADI with DMS specimens were dependent on variations in ausferrite and proeutectoid ferrite volume fractions and carbon content of high carbon austenite. In this specimens fatigue strength increases with increasing ausferrite volume fractions (**Fig. 13**). As mentioned before the AFVF increased with increasing ICAT and austempering temperature (Figs. 8–10). In the case of increasing AFVF the continuity of ausferrite structure along intercellular boundaries becomes more obvious (Figs. 8–10). The continuity of ausferrite structure plays an important role in determining of fatigue behavior of ADI with DMS. When continuity of ausferrite structures increases fracture pattern change from ductile to brittle.

As mentioned in section 3.1, ADI with DMS specimens, high carbon austenite volume fractions and its carbon content increases with increasing austenization and austempering temperature (see Figs. 5–6 and Table 2). Some authors[38,39] evaluated the fatigue strength of ADI by using $X_\gamma C_\gamma$ parameter where $X_\gamma$ stands for high carbon austenite volume fraction and $C_\gamma$ corresponds to austenite carbon content. In this study, the variation of fatigue strengths with parameter $X_\gamma C_\gamma$ is shown **Fig. 14**. This result is in good agreement with previous studies.[38,39]

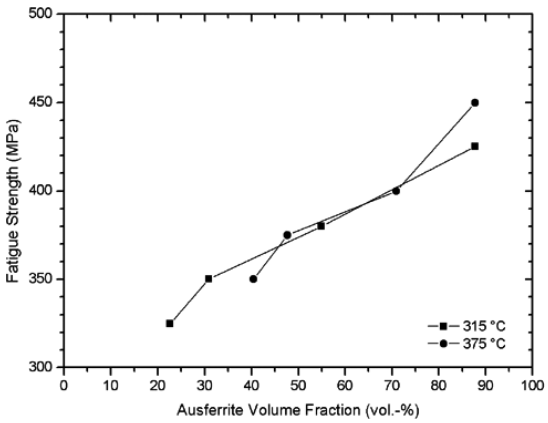


**Fig. 13.** Relationship between ausferrite volume fraction and fatigue strength.

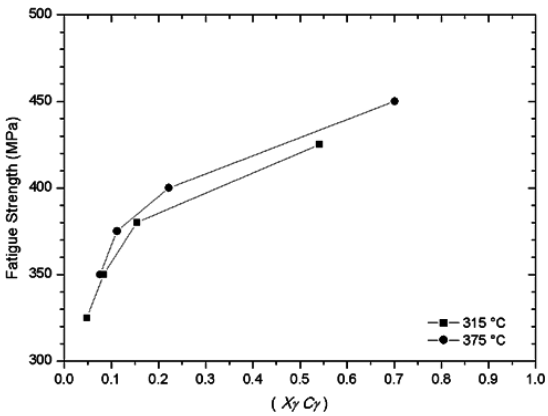


**Fig. 14.** Variation of fatigue strength with $X_\gamma C_\gamma$ parameter.

The effects of proeutectoid ferrite volume fraction (PFVF) on fatigue strength of specimens are given in **Fig. 15**. As can be seen from this figure fatigue strength decreases with increasing PFVF's. The lower fatigue strengths of specimens with high PFVF may be attributed to ductile nature of ferrite. The crack propagates preferably in ferrite.[20]

Conventionally austempered specimen at 900°C without proeutectoid ferrite exhibited higher fatigue strength than all those tested specimens. This result arose from the highest volume fraction of high carbon austenite and its carbon content (Figs. 5–6 and Table 2). Maximum fatigue strength was achieved with austempering treatments, which gave maximum high carbon austenite volume fraction.[38,39,48–50]

### 3.3. Fractographic Examinations

Fractographs of the ADI with DMS specimens are shown in **Fig. 16**. The graphite is generally a source a crack initi-

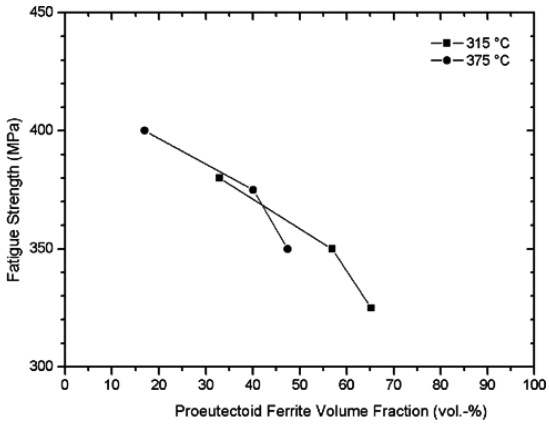


**Fig. 15.** Relationship between proeutectoid volume fraction and fatigue strength of specimens.

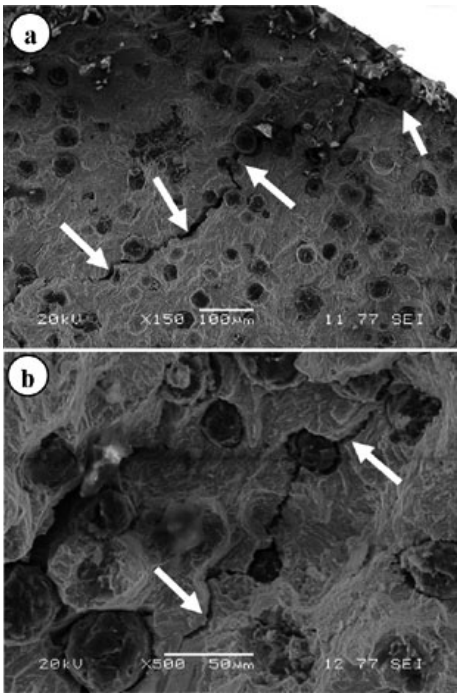


**Fig. 16.** SEM fractograph of the fatigue specimen 810-375. a) lower magnification and b) higher magnification. (Arrows indicate that crack path linking of graphite nodules).

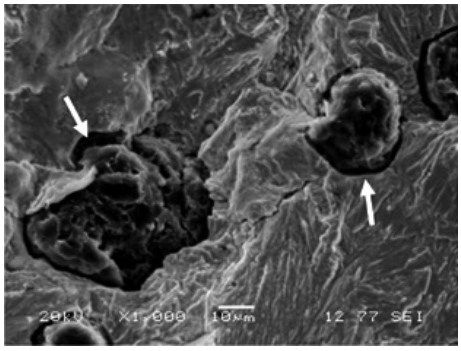


**Fig. 17.** SEM fractograph of the fatigue specimen 900-315. (Arrows indicate that decohesion between graphite nodules-matrix).

ation site since the brittle and low strength graphite acts as an inner crack in cast iron.[20] Graphite is a source for crack initiation (Fig.16(a)). Figure 16(b) shows that the crack propagation occurs by the linking of graphite nodules. The fatigue crack follows the path of least resistance through the matrix between nodules. Wade *et al*.[20] reported the similar crack propagation behavior in austempered ductile iron with duplex matrix.

Some decohesion between graphite-matrix interfaces and extensive crack branching was also observed (**Fig. 17**). Results of earlier studies support this fracture behavior of ADI.[31,32] Decohesion formation between graphite-matrix interfaces is attributed to mismatch in mechanical properties of graphite and matrix structure. Lin *et al*. reported that decohesion takes place at the graphite-matrix interfaces at low levels of strain of ADI.[32]

## 4. Conclusion

(1) By keeping the intercritical austenization and austempering time, the phase volume fractions in austempered ductile iron can be controlled preciously following austempering from intercritical austenitizing temperatures range.

(2) Fatigue strengths of austempered specimens increase with increase of ausferrite volume fraction and also $X_\gamma C_\gamma$ parameter.

(3) The continuity of ausferritic structure along intercellular boundaries plays an important role in determining fatigue behavior of ADI with DMS. In the case of increasing continuity of ausferritic structure, fracture pattern changed from ductile to brittle.

(4) Conventionally austempered specimens exhibited much greater fatigue strength than all specimens austempered from intercritical austenization temperatures ranges.

**Acknowledgement**

The authors are grateful for the financial support of this work by Gazi University Scientific Research Projects (Project No: GÜBAP 07/2005-25 and GÜBAP 07/2010-68).

## REFERENCES

1) R. C. Voigt, L. M. Eldoky and H. S. Chiou: *AFS Trans.*, **94** (1986), 645.
2) A. M. Rashidi and M. Moshrefi-Torbati: *Mater. Lett.*, **45** (2000), 203.
3) J. Aranzabal, G. Serramoglia and D. Rousiere: *Int. J. Cast. Met. Res.*, **16** (2003), 185.
4) V. Kilicli and M. Erdogan: *Mater. Sci. Technol.*, **22** (2006), 919.
5) V. Kilicli and M. Erdogan: *J. Mater. Eng. Perform.*, **19** (2010), 142.
6) Y. Sahin, V. Kilicli, M. Ozer and M. Erdogan: *Wear*, **268** (2010), 153.
7) M. Erdogan, V. Kilicli and B. Demir: *J. Mater. Sci.*, **44** (2009), 1394.
8) M. Erdogan, V. Kilicli and B. Demir: *Int. J. Mater. Res.*, **99** (2008), 751.
9) V. Kilicli and M. Erdogan: *J. Mater. Eng. Perform.*, **17** (2008), 240.
10) V. Kilicli and M. Erdogan: *Int. J. Cast. Met. Res.*, **20** (2007), 202.
11) Y. Sahin, M. Erdogan and V. Kilicli: *Mater. Sci. Eng. A.*, **444** (2007), 31.
12) A. D. Basso, R. A. Martinez and J. A. Sikora: *Mater. Sci. Technol.*, **25** (2009), 1271.
13) A. P. Cisilino, A. Basso, R. Martinez and J. Sikora: *Fatigue Fract. Eng. M*, **33** (2010), 1.
14) A. D. Basso, R. A. Martinez and J. A. Sikora: *Mater. Sci. Technol.*, **23** (2007), 1321.
15) A. Basso, R. Martínez and J. Sikora: *J. Alloys. Compd.*, **509** (2011), 9884.
16) T. Kobayashi and H. Yamamoto: *Metall. Mater. Trans. A.*, **19** (1988), 319.
17) T. Kobayashi and S. Yamada: *Metall. Mater. Trans. A.*, **27** (1996), 1961.
18) Z. R. He, G. X. Lin and S. Ji: *Mater. Charact.*, **38** (1997), 251.
19) M. Hafiz: *Z. Metallkd.*, **92** (2001), 1258.
20) N. Wade and Y. Ueda: *ISIJ Int.*, **20** (1980), 857.
21) M. Sofue, S. Okada and T. Sasaki: *AFS Trans.*, **86** (1978), 1173.
22) T. Watmaugh: *AFS Trans.*, **74** (1978), 742.
23) D. F. Socie and J. Fash: *AFS Trans.*, **90** (1982), 385.
24) D. Krishnaraj, K. V. Rao and S. Seshan: *AFS Trans.*, **97** (1989), 345.
25) G. P. Faubert, D. J. Moore and K. B. Rundman: *AFS Trans.*, **98** (1990), 759.
26) M. Grech and J. M. Young: *AFS Trans.*, **98** (1990), 345.
27) J. F. Janowak, A. Alagarsamy and D. Venugopalan: *AFS Trans.*, **98** (1990), 563.
28) G. P. Faubert, D. J. Moore and K. B. Rundman: *AFS Trans.*, **99** (1991), 563.
29) Y. Tanaka and H. Kage: *Mater. Trans. JIM*, **33** (1992), 543.
30) K. L. Hayrynen, D. J. Moore and K. B. Rundman: *AFS Trans.*, **100** (1992), 93.
31) L. Bartosiewicz, A. R. Krause, F. A. Alberts, I. Singh and S. K. Putatunda: *Mater. Charact.*, **30** (1993), 221.
32) C. K. Lin, P. K. Lai and T. S. Shih: *Int. J. Fatigue.*, **18** (1996), 297.
33) G. L. Greno, E. L. Pardo and R. E. Boeri: *AFS Trans.*, **98** (1998), 31.
34) J. Luo, R. A. Harding and P. Bowen: *Metall. Mater. Trans. A*, **33** (2002), 3719.
35) M. Tayanç, K. Aztekin and A. Bayram: *Mater. Design*, **28** (2007), 797.
36) S. Salman, F. Fındık and P. Topuz: *Mater. Design*, **28** (2007), 2210.
37) G. Toktaş, A. Toktaş and M. Tayanç: *Mater. Design*, **29** (2008), 1600.
38) P. Shanmugam, P. P. Rao, K. U. Rajendra and N. Venkataraman: *J. Mater. Sci.*, **29** (1994), 4933.
39) M. Bahmani, R. Elliott and N. Varahram: *J. Mater. Sci.*, **32** (1997), 5383.
40) C. K. Lin and J. Y. Wei: *J. Mater. Sci.*, **37** (2002), 709.
41) C. Verdu, J. Adrien and A. Reynaud: *Int. J. Cast. Met. Res.*, **18** (2005), 346.
42) A. Basso, M. Caldera, M. Chapetti and J. Sikora: *ISIJ Int.*, **50** (2010), 302.
43) K. W. Andrews: *JISI*, **203** (1965), 721.
44) B. D. Cullity: Elements of X-ray Diffraction, Addison-Wesley, Reading, MA, (1978), 411.
45) K. B. Rundman and R. C. Klug: *AFS Trans.*, **90** (1982), 499.
46) C. S. Roberts: *Trans. AIME*, **197** (1953), 203.
47) A. D. Basso and J. A. Sikora: *Int. J. Metalcast.*, **23** (2012), 7.
48) R. Kazerooni, A. Nazarboland and R. Elliot: *Mater. Sci. Technol.*, **13** (1997), 1007.
49) N. Darwish and R. Elliot: *Mater. Sci. Technol.*, **9** (1993), 572.
50) N. Darwish and R. Elliot: *Mater. Sci. Technol.*, **9** (1993), 882.
51) A. Trudel and M. Gagne: *Can. Metall. Q.*, **36** (1997), 289.